IEEE Access
Multidisciplinary ⋮ Rapid Review ⋮ Open Access Journal

Received November 22, 2020, accepted December 8, 2020, date of publication December 16, 2020, date of current version December 31, 2020.

Digital Object Identifier 10.1109/ACCESS.2020.3045158

Hybrid Power Quality Compensation System for Electric Railway Supplied by the Hypotenuse of a Scott Transformer

LEILEI ZHAO, (Graduate Student Member, IEEE), MINGLI WU, (Member, IEEE), QIUJIANG LIU, (Member, IEEE), PENG PENG, AND JING LI, (Member, IEEE)
School of Electrical Engineering, Beijing Jiaotong University, Beijing 100044, China

Corresponding author: Mingli Wu (mlwu@bjtu.edu.cn)

This work was supported in part by the Fundamental Research Funds for the Central Universities under Grant 2018YJS157.

ABSTRACT To solve the three-phase unbalance and reactive power problems in the electric railway power supply system, this paper proposes a Scott transformer based hypotenuse hybrid traction power system (Scott-HHPS). Compared with other co-phase traction power supply systems, the Scott-HHPS could achieve the same compensation objective with smaller active compensation capacity. The paper analyzes the basic principle and makes a comparison between the Scott-HHPS and typical co-phase power supply system. The mathematical relationships among the load current, power factor and capacity demand in condition of power factor variation and regenerative braking are analyzed. In order to further reduce the compensation capacity of the Scott-HHPS, the partial compensation strategy in respect to the index of power factor and unbalance is proposed. Besides, an instantaneous current detection method based on the theorem of conservation of power is adopted to simplify the control algorithms. Simulations and experiments are both constructed and the results demonstrate that the Scott-HHPS can effectively improve the power quality in the electric railway power supply system.

INDEX TERMS Electric railway, hybrid compensation, negative sequence current (NSC), power quality, Scott transformer.

I. INTRODUCTION

Electric railway has been playing significant roles in region connection, freight transportation, and economic development. There are still some concerned problems and challenges in power quality such as unbalance, reactive power and harmonics [1], [2]. In addition, in a traditional railway power supply substation, electricity is always transformed into two phases. The sections of phase splitting with isolation insulators seriously restrict the railway development towards high speed and heavy haul services.

Aiming for solving these problems, many schemes have been proposed and some were put into practice. The compensation methods based on the static var compensator (SVC) are discussed in [3], [4]. These passive methods can compensate reactive power and have the advantages of convenience of design, ease of application and low cost, but their response time cannot keep up with the requirement of dynamic compensation and even bring harmonic pollutions.

With the development of switching devices, the power quality problems caused by the nonlinear loads tend to be solved by the advanced power electronics technology. A railway static power conditioner (RPC) was proposed in [5], [6]. RPC was a pioneering innovation that excited many improvements in the traction power supply system later [7]–[18]. RPC can compensate for the negative sequence current and reactive power caused by the unbalanced loads of two feeders. Negative sequence compensation systems based on the three-phase voltage converter were proposed to improve the power quality of a traction substation [7], [8]. The railway hybrid power quality compensator (HPQC) with LC coupled branch were proposed which could operate in lower dc-link voltage [9]–[11]. A half-bridge-converter-based railway static power conditioner which can reduce half of the power switches was proposed [12]. Some high-power structures based on MMC were also proposed for railway power

The associate editor coordinating the review of this manuscript and approving it for publication was Alexander Micallef.

compensation [13]–[15]. The schemes integrate with special circuit modifications were proposed [16], [17]. References [9], [18]–[21] removed the neutral section at the exit of the traction substation, adopting single-phase feeding connection scheme by comparing with RPC. The two adjacent substations can supply in the same phase, so it was called co-phase system. The above researches all demonstrate that the compensation system based on the power electronic devices is an effective solutions to power quality problems of traction power supply system, but the capital cost restrict its wide application in practice.

Because the cost of passive devices is much lower than that of power electronics devices, some hybrid compensation schemes are proposed to reduce the total compensation costs. TCR, TSC and FC are typical representatives of passive devices, which are commonly used to compensate reactive power and filter low-order harmonics [22]–[26]. Magnetic controlled reactor (MCR) is also adopted instead of the traditional passive device [20], [21]. The table 1 summarizes the main characteristics of the SVC, RPC and co-phase compensation schemes in the railway power supply system.

TABLE 1. Comparisons between SVC, RPC and Co-phase schemes.

Items	SVC	RPC	Co-phase
Switching devices	Thyristor	IGBT	IGBT
Number of exit phase	2	2	1
Capability	Reactive power compensating and voltage regulation	Load balancing and harmonics filtering	Load balancing and harmonics filtering
Cost	Low	High	High
Response time	0.1~0.2s	0.02s	0.02s

Summarizing above researches, a great demand of load active power is still needed to balance the three-phase currents even though the reactive power has been compensated. It would be advantageous if the required active power can be smaller, and hence the capacity of active devices can be decreased accordingly. This paper proposes a Scott transformer based hypotenuse hybrid traction power system (Scott-HPSS), whose structure is shown in Fig. 1. The capacity demand for active devices of Scott-HPSS is significantly decreased by 29.3% compared with that of typical co-phase power supply system. Furthermore, as the Scott-HPSS takes only the hypotenuse voltage of the Scott transformer supplying the loads, there will be no phase split at the exit of the traction substation.

In order to explore the feasibility of the Scott-HPSS in practice, the overall analysis of capacity demand is primarily carried out. The compensation capacity is mostly designed under the condition of a fixed locomotive power factor [26], [27], actually which cannot cover all load power

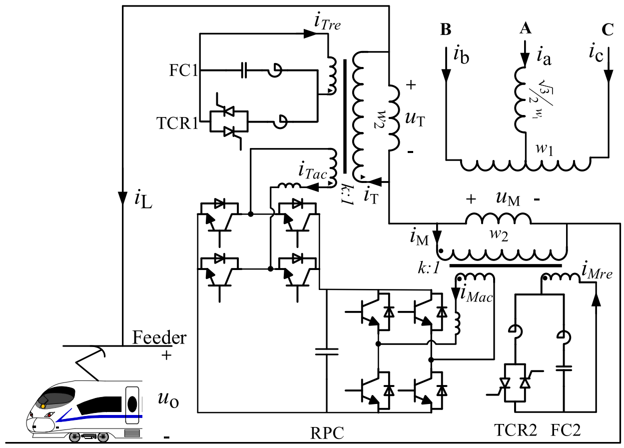

FIGURE 1. Structure of the Scott-HHPS.

scenario. The compensation capacity under the condition of regenerative braking is seldom discussed either. So in consideration of power factor variation and regenerative braking, this paper analyzes the compensation principle and capacity demand under the full compensation in detail. As full compensation is not always required in reality, the partial compensation strategy in terms of power quality index is also developed, which could further reduce the capacity demand of compensation devices. Particularly, relying on the characteristics of Scott transformer, a new current detection method is proposed to simplify the algorithms, and the method can also be applied to other balanced transformers.

This paper is organized as follows. The system structure and comparisons with typical structure of co-phase system are discussed in section II. In section III, the compensation principle and capacity demand under full and partial compensation are analyzed. A method to design a controller of current detection is proposed in section IV. Simulation and experiment results are presented to validate the feasibility of the proposed topology and the control algorithms in section V. Finally, the conclusion is given in section VI.

II. SCOTT TRANSFORMER BASED HYPOTENUSE HYBRID TRACTION POWER SYSTEM

A. BASIC STRUCTURE

As illustrated in Fig. 1, the 220-kV three-phase voltages are transformed into two 27.5kV orthogonal single-phase power sources through the Scott transformer. The Scott transformer is a kind of balanced transformer which is physically made up of two single-phase transformers, simply named T and M phase transformer. The secondary windings of T and M phase transformer are connected in series and jointly feed the traction loads across the hypotenuse voltage u_o. For adapting to the voltage rating of the power electronic devices, two secondary voltages of T and M phase transformer are stepped down by each isolation transformer.

The active compensation part is composed of a pair of back-to-back H-bridge converters which are connected via the common dc-link. These two H-bridge converters can transfer active power from one ac side to the other and they can also compensate the difference of reactive power between the reference and the generated by the passive branches. The passive compensation part is constituted of two sets of TCR and FC, which could output a certain range of reactive power from inductive to capacitive. The capacitor banks with the help of series reactors can be tuned to filter third, fifth and higher-order harmonics as a high-pass filter.

The equivalent circuit model of the system is depicted in Fig. 2. $\boldsymbol{U}_T, \boldsymbol{U}_M$ are the secondary voltages of T and M phase transformer, $\boldsymbol{I}_T$ and $\boldsymbol{I}_M$ are currents flowing through the secondary windings of T and M transformer. $\boldsymbol{Z}_{sT}$ and $\boldsymbol{Z}_{sM}$ are the sum of secondary side impedance of the system sources and Scott transformer. Converters fed by $\boldsymbol{U}_T$ and $\boldsymbol{U}_M$ voltages could be considered as two controllable current sources and they output currents $\boldsymbol{I}_{Tac}$ and $\boldsymbol{I}_{Mac}$ respectively. The equivalent output currents of passive TCR + FC branches are $\boldsymbol{I}_{Tre}$ and $\boldsymbol{I}_{Mre}$ respectively. $\boldsymbol{U}_o$ is the voltage of the power supply arm, $\boldsymbol{Z}_L$ and $\boldsymbol{I}_L$ are equivalent load impedance and traction current.

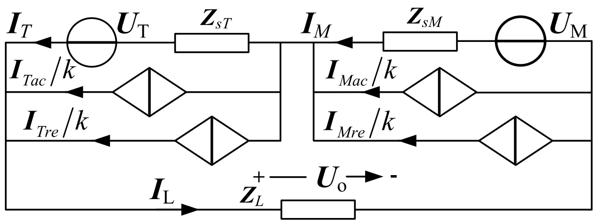

FIGURE 2. Equivalent circuit model of the Scott-HPSS.

The equations of the Scott-HPSS based on the Kirchhoff's current and voltage laws are as follows:

$$\boldsymbol{U}_o = \boldsymbol{U}_T + \boldsymbol{U}_M, \tag{1}$$

$$\begin{cases} \boldsymbol{I}_T = \boldsymbol{I}_L - \dfrac{\boldsymbol{I}_{Tac} + \boldsymbol{I}_{Tre}}{k} \\ \boldsymbol{I}_M = \boldsymbol{I}_L - \dfrac{\boldsymbol{I}_{Mac} + \boldsymbol{I}_{Mre}}{k}. \end{cases} \tag{2}$$

where k is the ratio of isolation transformers. To achieve active power exchange and reactive power compensation, the output currents $\boldsymbol{I}_{Tac}$, $\boldsymbol{I}_{Mac}$, $\boldsymbol{I}_{Tre}$, $\boldsymbol{I}_{Mre}$ will be regulated integrally to eventually realize grid balance.

B. COMPARISONS WITH TYPICAL CO-PHASE POWER SUPPLY SYSTEM

The co-phase schemes of railway traction power supply system take only one secondary voltage port of the traction transformer supplying the loads, and the other port is connected to active compensation devices. Scheme in [9] is a typical representative of co-phase power supply system with balanced transformer. Fig. 3 shows the profile of this type of structure, marked with the symbol ∟ for convenience. The hypotenuse structure in this paper is marked with the symbol ∠. Compared with ∟, ∠ structure has three features as following comments:

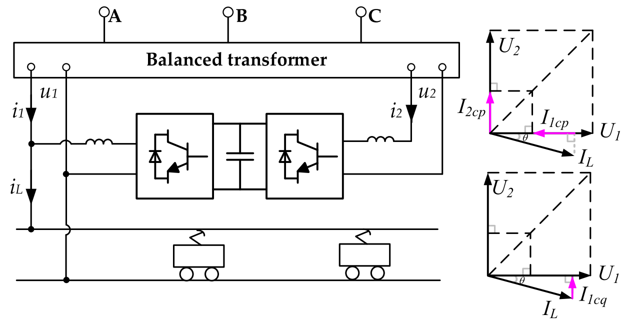

FIGURE 3. Topology of the ∟ type co-phase power supply system and its phasor diagram.

1) VOLTAGE RATING

In ∟ structure, because the supply arm voltage is supplied by the secondary port of a traction transformer, the secondary voltages are exactly the voltage of the supply arm 27.5kV. However ∠ structure requires a lower voltage level by $1/\sqrt{2}$ on account of the series connection of secondary ports of the traction transformer. So the voltage level of compensation devices and insulation requirements are reduced accordingly.

2) COMPENSATING CURRENTS

Fig. 3 shows the phasor diagram of ∟ structure. Taking voltage port 2 for the locomotives, under the condition of full compensation, the amplitudes of active compensating currents $\boldsymbol{I}_{1cp}$ and $\boldsymbol{I}_{2cp}$ are equal and equivalent to the half of the load active current. The reactive compensating current of M phase $\boldsymbol{I}_{1cq}$ is exactly the whole load reactive current and there is no need for reactive compensating current in port 1.

The detailed compensation principle of ∠ structure will be analyzed in next section. It reveals that the amplitudes of active compensating currents $\boldsymbol{I}_{Tcp}$ and $\boldsymbol{I}_{Mcp}$ are still equal but equivalent to the half of difference of the active currents in T and M phase. Comparing with ∟ structure, the active compensating current is much less, and the reactive compensating current is larger. Particularly when the power factor angle of the load becomes zero, there is no need to compensate any amount of active current in ∠ structure.

3) TOTAL COMPENSATING CAPACITY

Fig. 4 shows a comparison of total compensating capacity versus power factor angle θ (in radians) of the locomotives between the ∟ and ∠ structure. Take the apparent power of the load as the base value, it can be seen that in the range of θ from 0 to $\pi/4$, the average compensation capacity of T and M phase of ∠ type is always smaller than that of ∟ type, which means ∠ type structure has the superiority of low compensation capacity to achieve the same performance.

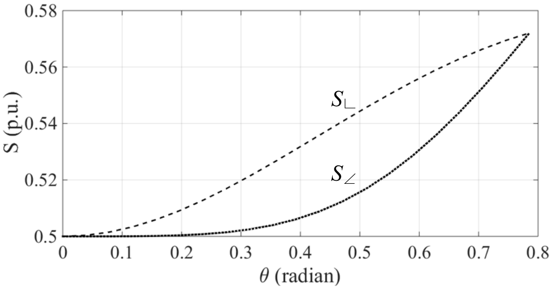

FIGURE 4. Compensating capacity demand versus θ between ⌊ and ∠ type structure.

III. COMPENSATION PRINCIPLE AND CAPACITY DESIGN

A. PRINCIPLE OF COMPENSATION

Take $\boldsymbol{U}_{\mathrm{A}}$ as the reference phasor, and a reference frame of voltage could be defined as (3), the supply arm voltage $\boldsymbol{U}_{\mathrm{o}}$ lags behind $\boldsymbol{U}_{\mathrm{A}}$ by $\pi/4$.

$$\begin{cases}\boldsymbol{U}_A = U, \boldsymbol{U}_B = Ue^{-j\frac{2\pi}{3}}, \boldsymbol{U}_C = Ue^{j\frac{2\pi}{3}} \\ \boldsymbol{U}_T = \frac{\sqrt{3}}{K}U, \boldsymbol{U}_M = \frac{\sqrt{3}}{K}Ue^{-j\frac{\pi}{2}}, \boldsymbol{U}_o = \frac{\sqrt{6}}{K}Ue^{-j\frac{\pi}{4}}\end{cases} \tag{3}$$

where U is the rms value of primary three-phase voltages. $\mathrm{K} = \mathrm{w}_1/\mathrm{w}_2$, w_1 and w_2 are turns of primary and secondary windings of its M phase transformer.

As shown in Fig. 2, when no compensation, the phasor diagram including three-phase currents under the running condition is shown in Fig. 5(a). The load current $\boldsymbol{I}_L$ completely flows through the secondary windings of T and M phase transformer, which means $\boldsymbol{I}_T = \boldsymbol{I}_M = \boldsymbol{I}_L$. At this time, $\boldsymbol{U}_T, \boldsymbol{I}_T$ and $\boldsymbol{U}_M, \boldsymbol{I}_M$ are not in phases. The active and reactive current flowing through the T phase are $\boldsymbol{I}_{Tp}$ and $\boldsymbol{I}_{Tq}$ (lagging) respectively. The active and reactive current acorss the winding of M phase are $\boldsymbol{I}_{Mp}$, $\boldsymbol{I}_{Mq}$ (leading). They have relationships as below

$$\begin{cases}\boldsymbol{I}_T = \boldsymbol{I}_{Tp} + \boldsymbol{I}_{Tq} = I_u - jI_v \\ \boldsymbol{I}_M = \boldsymbol{I}_{Mp} + \boldsymbol{I}_{Mq} = -jI_v + I_u,\end{cases} \tag{4}$$

where

$$\begin{cases}I_u = I_L \sin\left(\frac{\pi}{4} - \theta\right) \\ I_v = I_L \cos\left(\frac{\pi}{4} - \theta\right).\end{cases} \tag{5}$$

Ignoring the harmonic components, I_L is the rms value of the fundamental component of the load current. Three-phase currents on the primary side of Scott transformer is expressed as

$$\begin{cases}\boldsymbol{I}_A = \sigma I_L e^{-j\theta} \\ \boldsymbol{I}_B = \frac{\left(\sqrt{3}-1\right)\sigma}{2} I_L e^{-j\theta} \\ \boldsymbol{I}_C = -\left(\boldsymbol{I}_A + \boldsymbol{I}_B\right).\end{cases} \tag{6}$$

where $\sigma = 2/\sqrt{3}\,K$. The three-phase currents is co-linear and the unbalance degree of primary currents equals to 1.

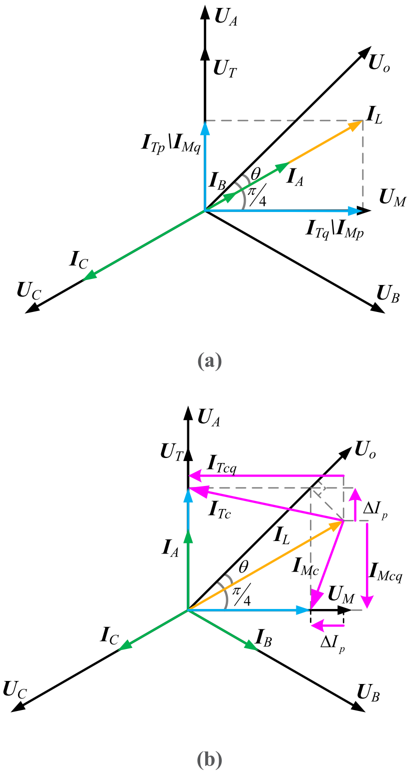

FIGURE 5. Phasor diagram of voltages and currents in grid and secondary side: (a) without compensation; (b) with compensation.

It is necessary to compensate a certain amount of active and reactive power to realize three-phase balance. Fig. 5(b) shows the current phasor diagram after full compensation, $\boldsymbol{I}_{Tc}$ and $\boldsymbol{I}_{Mc}$ are total compensation currents for T and M phase respectively under the condition of full compensation.

The active portion of compensation currents of T and M phases are $\boldsymbol{I}_{Tcp} = \Delta I_p$ and $\boldsymbol{I}_{Mcp} = j\Delta I_p$. According to equation (5), the amount of transferred active current ΔI_p is

$$\Delta I_p = \frac{1}{2}\left(I_{Mp} - I_{Tp}\right) = \frac{1}{\sqrt{2}} I_L \sin(\theta). \tag{7}$$

The back-to-back H-bridge converters can be controlled as a channel to transfer half of the difference of I_{Tp} and I_{Mp} to equalize the active power of the two secondary phases. After the active currents are compensated, the unbalance degree of primary side currents has been reduced but not to 0. It is still necessary for reactive power to be compensated. The value of reactive currents to be compensated for the two phases are $\boldsymbol{I}_{Tcq} = jI_v$ and $\boldsymbol{I}_{Mcq} = -I_u$ according to the equation (4). Eventually the three-phase currents in the grid side are changed into

$$\begin{cases}\boldsymbol{I}_A = \frac{\sigma\cos\theta}{\sqrt{2}} I_L \\ \boldsymbol{I}_B = \frac{\sigma\cos\theta}{\sqrt{2}} I_L e^{-j\frac{2\pi}{3}} \\ \boldsymbol{I}_C = \frac{\sigma\cos\theta}{\sqrt{2}} I_L e^{j\frac{2\pi}{3}}.\end{cases} \tag{8}$$

The three-phase currents become balanced after compensation. It can be seen that the amplitude of currents is proportional to the active load current, because only active power is supplied by the three-phase sources. The above calculation results are also reasonable in braking conditions, when I_L is a negative and the load current is fed back into the grid. Whatever conditions, the compensation devices at T and M phases work together to realize the comprehensive treatment of negative sequence and reactive power of the power grid.

B. CAPACITY ANALYSES

At present, locomotives with AC-DC driven are running together with AC-DC-AC driving locomotives on many lines [28], so the power factor in traction substations are not always unitary. In previous literatures [26], [27], in order to characterize the power consumption, analyses of compensation capacity directly presuppose power factor to be the value of calculation results from the 95% probability value of active power and reactive power. But the assumption may not reveal the poor operating condition for a general substation and is not distinct for observing a full-scale impact of the continuous changing of the loads on the capacity design. And in the analyses, the compensation capacity under the regenerative braking is not considered either. Actually in braking condition, some compensation settings for running condition would even degrade the power quality of the three-phase grid [29], so the regenerative braking situation should also be taken into account into capacity design.

1) FULL COMPENSATION

As for wider adaptability, the power factor angle of locomotives θ is assumed to vary from 0 to $\pi/4$ to stimulate the two common kinds of locomotives. The secondary active and reactive power compensation demand of T and M phase are calculated as equation (9) and (10).

$$\begin{cases} P_{Tc} = U_T I_{Tcp} = \dfrac{\sqrt{3}}{K} U \times \Delta I_p \\ P_{Mc} = -U_M I_{Tcp} = -\dfrac{\sqrt{3}}{K} U \times \Delta I_p, \end{cases} \tag{9}$$

$$\begin{cases} Q_{Tc} = -U_T I_{Tcq} = -\dfrac{\sqrt{3}}{K} U \times I_v \\ Q_{Mc} = U_M I_{Mcq} = \dfrac{\sqrt{3}}{K} U \times I_u. \end{cases} \tag{10}$$

The sign '+' of P states the active power is absorbed by the compensation system, '-' states the active power is generated by the compensation system. The sigh '+' of Q means the compensation device of T or M phase behaves like a capacitive source and '-' means it behaves like an inductive source. Under running conditions, I_L is a positive number and in braking states, I_L is a negative number. Fig. 7. shows the relationships of compensation power demand in T and M phase versus I_L and θ in full compensation condition. Take the maximum power of the load as a base value and the maximum braking current is presumed to be 0.75 times of the maximum running current [30].

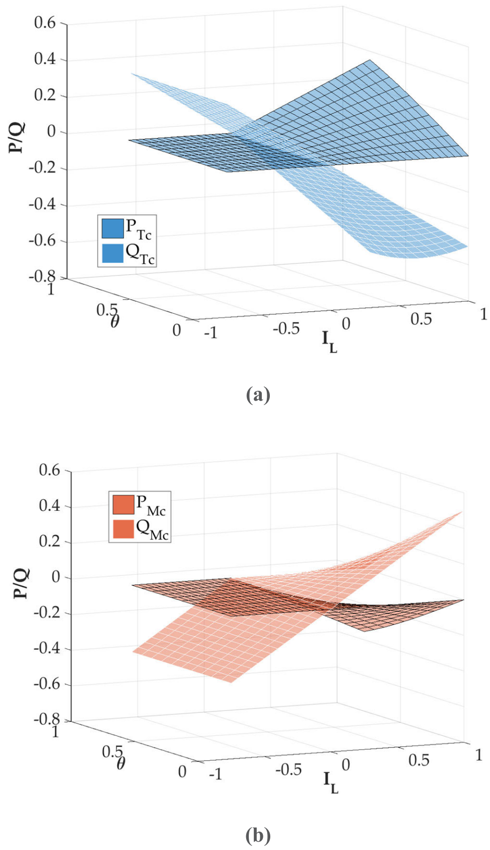

FIGURE 6. **Compensation capacity demand in: (a) phase T; (b) phase M.**

Fig. 6(a) shows the compensation power demand of T phase. The maximum transferred active power occurred at $(I_L, \theta) = (1, \pi/4)$ with value of 0.35 under running condition ($I_L > 0$). Demand of reactive power compensation increase with the rising of load current, and reaching a negative maximum value of -0.71 at the point (1, $\pi/4$). In braking condition ($I_L < 0$), there is no active power to be compensated since only PWM-controlled locomotives have the capability of regenerative breaking and their power factor angle always keeps 0. At this time, the direction of load current is reversed and begins injecting into the power grid. The lagging reactive current in running condition is converted to the leading one, so the reactive compensation should be replaced with some inductive current.

Fig. 6(b) shows the variation of compensation power demand of the M phase. The active power delivered via dc capacitor is completely opposite to that in (a), because the active power is conservative. It reaches the maximum value of -0.35 at (1, $\pi/4$). But the maximum value of reactive power compensation demand occurs at $(I_L, \theta) = (1, 0)$ with 0.5. In braking condition, the load reactive current gets zero, and there is no need to transfer the active power either. The amount of reactive power decreases to a limit which depends on the maximum braking current.

According to the above analysis, it is obvious that the amount of compensation power of T and M phase have asymmetrical range and except for structural reasons, it also depends on the braking current coefficient. The passive branches of Scott-HPSS should meet both the power compensation demands in running and braking condition. So the rating of the TCR's capacity is designed larger than the rating of the capacitor's by an amount to provide the maximum lagging vars that have to be absorbed from the system. For T phase, the capacities of FC1 and TCR1 are written as following respectively.

$$\begin{cases} |Q_{FC1}| = \dfrac{\sqrt{3}U}{K} I_{\max} \\ Q_{TCR1} = |Q_{FC1}| + \dfrac{\sqrt{6}U}{2K} \eta_{\max} I_{\max}, \end{cases} \tag{11}$$

where η_{max} is the maximum braking current coefficient.

For M phase, the capacities of FC2 and TCR2 are respectively:

$$\begin{cases} |Q_{FC2}| = \dfrac{\sqrt{6}U}{2K} \eta_{\max} I_{\max} \\ Q_{TCR2} = |Q_{FC2}| + \dfrac{\sqrt{6}U}{2K} I_{\max}. \end{cases} \tag{12}$$

The capacity demand of back to back converters is designed in formula (13) based on the maximum capacity demand, which could meet both the active power compensation demand in the condition of barking and varying power factor from 0 to $\pi/4$.

$$S_{RPC} = \frac{\sqrt{2}}{4} S_{\max}. \tag{13}$$

S_{max} is the maximum apparent power of the load. Within the same range of power factor angle and braking condition, the minimum active compensating capacity demand of ∟ structure is as much as $\frac{1}{2}S_{max}$. As a comparison ∠ structure could effectively reduce the capacity of active compensation section by 29.3%. In practical application, considering that the residual margin of the active devices could provide fast dynamic reactive power as a supplement for the passive branches. The designing capacity of active devices can be appropriately enlarged according to the actual situation

2) PARTIAL COMPENSATION

In practical applications, full compensation is not often required, so it is significant to propose a partial compensation strategy that satisfies the indexes of the power quality. The partial compensation strategy can be summarized as a strategy with reactive power compensation prior to the negative sequence current compensation. The power factor λ is a reflection of reactive power in the grid side. In view of the secondary side [31], λ can be expressed as

$$\lambda = \cos\left(\tan^{-1} \frac{Q_L + (Q'_{Mc} + Q'_{Tc})}{P_L}\right), \tag{14}$$

P_L, Q_L is the active and reactive power of the load. As the compensation system will not change the total amount of active power, only reactive power can be compensated to satisfy the requirement of power factor. The superscript means the variables belongs to the partial compensation, and Q'_{Mc},Q'_{Tc} is the partially compensated power for T and M phase. Specially, full compensation corresponds to $\lambda = 1$, when $Q'_{Mc} + Q'_{Tc} = Q_{Mc} + Q_{Tc} = Q_L$. As for an expected power factor of λ_r, the capacity demand in partial compensation and full compensation have a relationship

$$(Q'_{Mc} + Q'_{Tc}) = \tan\left(\cos^{-1}\lambda_r\right) P_L + (Q_{Mc} + Q_{Tc}). \tag{15}$$

The above relationship only regulates the sum of Q'_{Mc},Q'_{Tc}. So define μ as a distribution factor of reactive power compensation, the partial compensation capacity Q'_{Mc}, Q'_{Tc} are written as (16). It is very meaningful to find a value of μ to minimize negative sequence currents.

$$\begin{cases} Q'_{Tc} = Q_{Tc} + \mu \tan\left(\cos^{-1}\lambda_r\right) P_L \\ Q'_{Mc} = Q_{Mc} + (1-\mu)\tan\left(\cos^{-1}\lambda_r\right) P_L. \end{cases} \tag{16}$$

Assume that the unbalanced active current have been fully transferred via the active compensation part, the residual reactive currents in phase T and phase M after partial compensation become

$$\begin{cases} I'_{Tq} = \dfrac{Q'_{Tc} + Q_T}{U_T} = \mu\sqrt{2}\tan\left(\cos^{-1}\lambda_r\right) \\ I'_{Mq} = \dfrac{Q'_{Mc} + Q_M}{U_M} = (1-\mu)\sqrt{2}\tan\left(\cos^{-1}\lambda_r\right). \end{cases} \tag{17}$$

The power factors of T and M ports are current ratios of their active portion and the sum values. They are respectively denoted as φ'_T and φ'_M and expressed as

$$\begin{cases} \varphi'_T = \tan^{-1}\left(\frac{I'_{Tq}}{I_{Tp}+\Delta I_p}\right) = \sqrt{2}\mu\tan\left(\cos^{-1}\lambda_r\right) \\ \varphi'_M = \tan^{-1}\left(\frac{I'_{Mq}}{I_{Mp}-\Delta I_p}\right) = \sqrt{2}(1-\mu)\tan\left(\cos^{-1}\lambda_r\right). \end{cases} \tag{18}$$

In balanced transformers, when power factors of two port loads are equal, the negative sequence currents generated by the two port loads weaken each other. So we let $\varphi'_T = \varphi'_M$, it leads to a distribution factor μ= 0.5, which is exactly the number that could reduce the negative current to the maximum extent.

IV. CONTROL ALGORITHM OF THE SCOTT-HPSS

In order to detect active and reactive portion of the load current, single phase current detection method is adopted. It always requires an orthogonal single generation (OSG) block to provide the orthogonal component of the load current in static frame. OSG is implemented using phase shift methods such as Hilbert transform, time delay, all pass filter, and SOGI. No matter what method is used, the delay of creating $\pi/2$ phase shift will slow down the dynamic response of the control system. But in this paper the method of the load current detection abandons the traditional OSG block and generates the reference currents in view of the whole three-phase system.

In the Scott traction power system, the secondary voltage of T transformer is in quadrature with that of M transformer. Since Scott transformer is a kind of balanced transformer, with equal voltage amplitude and $\pi/2$ phase displacement, the voltages and currents of Scott secondary ports could be seen as naturally Clark transformation from the primary side. So we take directions of u_T and u_M as static orthogonal reference frame, as they could constitute a rotating voltage vector, which is written as follows, j is imaginary unit

$$\boldsymbol{u}^{j\omega t} = \cos(\omega t) - j\sin(\omega t). \tag{19}$$

Assuming the load current only contains fundamental component and is defined as

$$i_L = \sqrt{2}I_L \cos\left(\omega t - \frac{\pi}{4} - \theta\right) \tag{20}$$

i_L has a power angle θ lagging of the supply arm voltage u_o. If no compensation, there would be $i_T = i_M = i_L$. Because the Scott-HPSS is a three-phase to single-phase system, based on the theorem of power conservation, the active and reactive power of the load are equivalent to that of three-phase. Hence it could be obtained through the matrix below on the basis of the theory of instantaneous reactive power.

$$\begin{bmatrix} i_p \\ i_q \end{bmatrix} = \begin{bmatrix} \cos\omega t & \sin\omega t \\ \sin\omega t & -\cos\omega t \end{bmatrix} \begin{bmatrix} i_T \\ i_M \end{bmatrix} = \begin{bmatrix} \bar{i}_p \\ \bar{i}_q \end{bmatrix} + \begin{bmatrix} \tilde{i}_p \\ \tilde{i}_q \end{bmatrix}. \tag{21}$$

The dc components of i_p and i_q respectively correspond to the rms value of active and reactive load currents and they are

$$\begin{cases} \bar{i}_d = I_L \cos\theta \\ \bar{i}_q = I_L \sin\theta. \end{cases} \tag{22}$$

Compared to conventional current detection method [15], utilization of inherent orthogonality of balanced transformer and theorem of power conservation could save three steps in conventional control algorithms, including OSG block of voltage u_T and u_M and detection of the arm supply voltage u_o. Hence the overall calculation burdens could be reduced and the calculation speed could be increased during each sampling period.

Because in the compensation system, the tasks of active and reactive are performed by different devices separately, the reference current of T and M phase converter i^*_{Tcp}, i^*_{Mcp} could be written as (23) according to Fig. 6(b) and equation (6). The minus denotes the M converter is sending out the active power.

$$\begin{cases} i^*_{Tcp} = \sqrt{2} \times \Delta I_p \times \cos\omega t = \bar{i}_q \times \cos\omega t \\ i^*_{Mcp} = -\sqrt{2} \times \Delta I_p \times \sin\omega t = -\bar{i}_q \times \sin\omega t. \end{cases} \tag{23}$$

The dc-link voltage of the capacitor in back-to-back converters should be stable to maintain the normal operation of the system. Tracking error between the voltage reference u_{dc_r} and the detected dc-link voltage u_{dc} is sent to a proportional-integral (PI) regulator to compensate the consumed active power. Current regulation after PI voltage controller together with i^*_{Tcp}, i^*_{Mcp} constitute the reference current i^*_{Tac}, i^*_{Mac} for the back-to-back converters. The reference current detection algorithm is shown in Fig. 7.

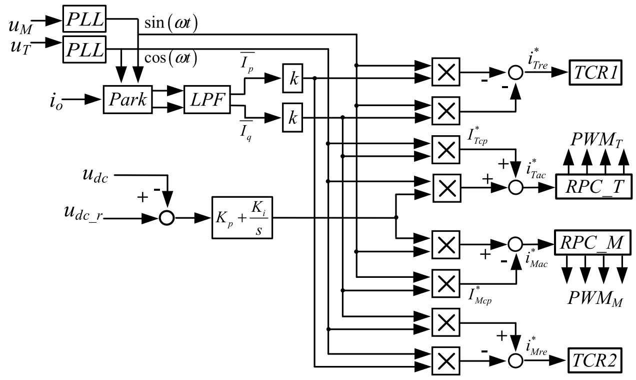

FIGURE 7. Reference current detection algorithm.

Based on the analysis in section III.A, the amplitude of reference reactive current for TCRs I^*_{Tre}, I^*_{Mre} could be seen as an addition and a subtraction of two components respectively

$$\begin{cases} I^*_{Tre} = -I_v \times \sin\omega t = -\left(\bar{i}_p + \bar{i}_q\right) \times \sin\omega t \\ I^*_{Mre} = I_u \times \cos\omega t = \left(-\bar{i}_p + \bar{i}_q\right)\cos\omega t. \end{cases} \tag{24}$$

The current differences between reference and actual current of the passive branches could be sent to RPC to slightly make up for the relatively low response speed of passive branches. The current control of the TCR is performed through the control of firing angle.

V. SIMULATION AND EXPERIMENTAL RESULTS

A. SIMULATION RESULTS

To further verify the feasibility of proposed system and control algorithms, simulations are carried out by Matlab/Simulink. Three different load scenarios are separately modeled with a resistor, inductor-resistor and current source. Simulations consist of two parts. The first part is to prove the proposed system and the control algorithm, and the second part makes a performance comparison with ∟ type structure. The detailed simulation parameters are shown in Table 2.

To assess the compensation performance of the Scott-HPSS system, three different load cases are set to represent different operating conditions. Case 1 is set according to the PWM-controlled locomotives with $P_L = 8MW$, $Q_L = 6Mvar$, $\theta = 0°$. Case 2 simulates the locomotive that has a low power factor with $P_L = 8MW$, $Q_L = 6Mvar$, $\theta = 36.87°$. Case 3 simulates the condition of regenerative braking with $P_L = -4MW$. Fig. 8 (a)(b)(c)(d) show the waveforms of the three-phase grid voltages and three-phase currents of case 1, 2 and 3 separately. Before 0.1s, there is no compensation, and the compensation system is put into work at 0.1s. After nearly a quarter cycle, the reference signal could be tracked

TABLE 2. Simulation parameters.

Items	Value
Line-voltage of three-phase sources	220kV
Turns ratio of Scott transformer	$220{:}\,27.5/\sqrt{2}$
Turns ratio of isolation transformers	$27.5/\sqrt{2}:1$
DC-link capacitance	20mF
DC-link reference voltage	2800V
Proportional gain	0.005
Integral gain	0.00001
Filter inductances	2mH
Rating of TCR1+FC1	9+7Mvar
Rating of TCR2+FC2	7+2Mvar
Sample frequency	10kHz

and the compensation system achieves good compensation performance in reactive and unbalanced current.

In Fig. 8(b), the load of case 1has unitary power factor. It can be seen there is amounts of unbalance and reactive power without compensation, but after 0.1s three-phase currents get compensated and they are balanced and in phase with three-phase voltages.

In Fig. 8(c), during 0∼0.1s the current waveforms are similar to that of case 1, but their phases are little shifted backwards. The compensation results after 0.1s are same with that of case1, because only active power are absorbed from three-phase power grid after compensation.

Fig. 8(d) simulates the regenerative condition of the load, there is braking energy fed back to the power system. When no compensation, the direction of the three-phase currents is completely inversed with the direction of case 1 and case 2. During 0.1∼0.3s the unbalance and reactive currents have been compensated and only the active portion of the load current is injected into the three-phase power system via the Scott transform. The current waveforms are opposite to that in case 1 and case 2 and their amplitudes reduce by as much as half of the value in case 1 and 2.

Fig. 9(a) shows the traction supply voltage u_o and load current i_L in case 2 with lagging power factor angle of 36.87°. Fig. 9(b) is the corresponding three-phase currents adopting ∟ type structure. Fig. 10 shows the calculation results of compensation power for case 2 in ∠ and ∟ structure. Fig. 10(a) is the result of ∟ structure with T phase arm supplying the load. At 0.1s, the compensating system is set to work. It can be seen that when the system reaches the steady state, the delivered active power from the T phase to M phase is about 4MW. Reactive power compensated in T phase is -6Mvar and 0 in M phase. There is no reactive power compensation of M phase and the results verify the above analyses.

Compared with the ∟ structure, the compensated active power of ∠ structure is 3MW, smaller than that in Fig. 10(b). In fact with the increasing of power factor, the amount of active compensation capacity gap between the two structures will be larger. The reactive power compensated in T phase is -7Mvar and 1Mvar in M phase. Although the sum of

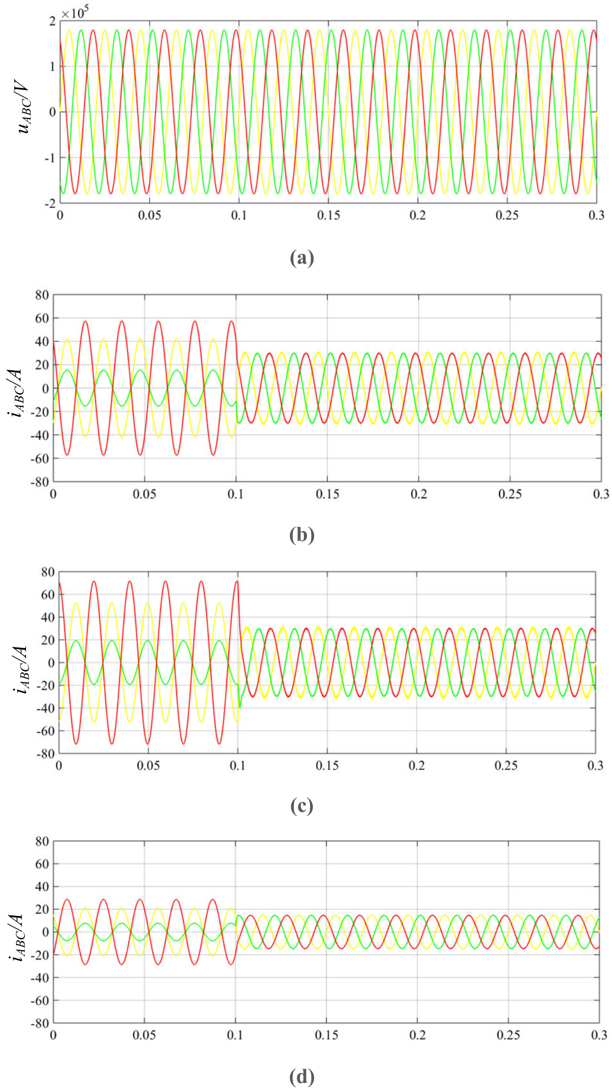

FIGURE 8. Three-phase voltages and currents of ∠ Scott-HPSS: (a) three-phase voltages; (b) three-phase currents in case 1; (c) three-phase currents in case 2; (d) three-phase currents in case 3.

reactive power need to be compensated is larger than that of ∟ structure, the reactive power could be compensated by passive devices instead of active devices. So it means Scott-HPSS system has a cost advantage due to the smaller active capacity demand and substitutability of the expensive power electronics.

B. EXPERIMENTAL RESULTS

An experimental setup rated at 2kVA has been built in the laboratory. A resistor (R) and a resistor-inductor (RL) load are adopted to represent two kinds of actual traction loads. The experimental setup is supplied by a three-phase power network simulator and it next connects to a Scott transformer. Then an isolation transformer in phase T of the Scott transformer is employed for electrical isolation. Table 3 gives the specifications of experimental parameters.

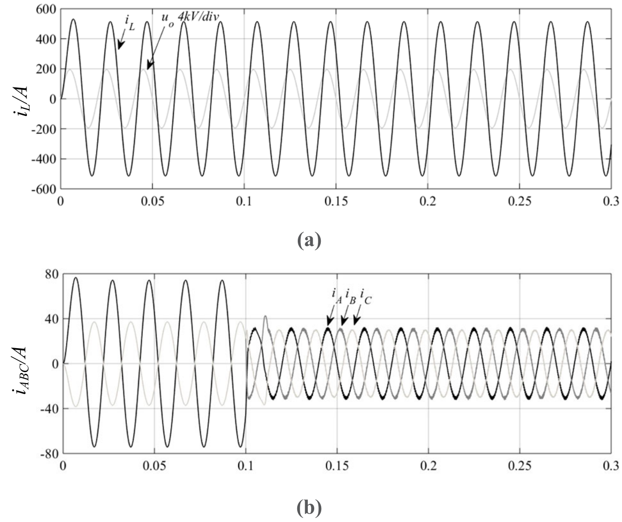

FIGURE 9. Voltages and currents waveforms of ⌞ structure: (a) traction arm voltage and load current; (b) three-phase currents.

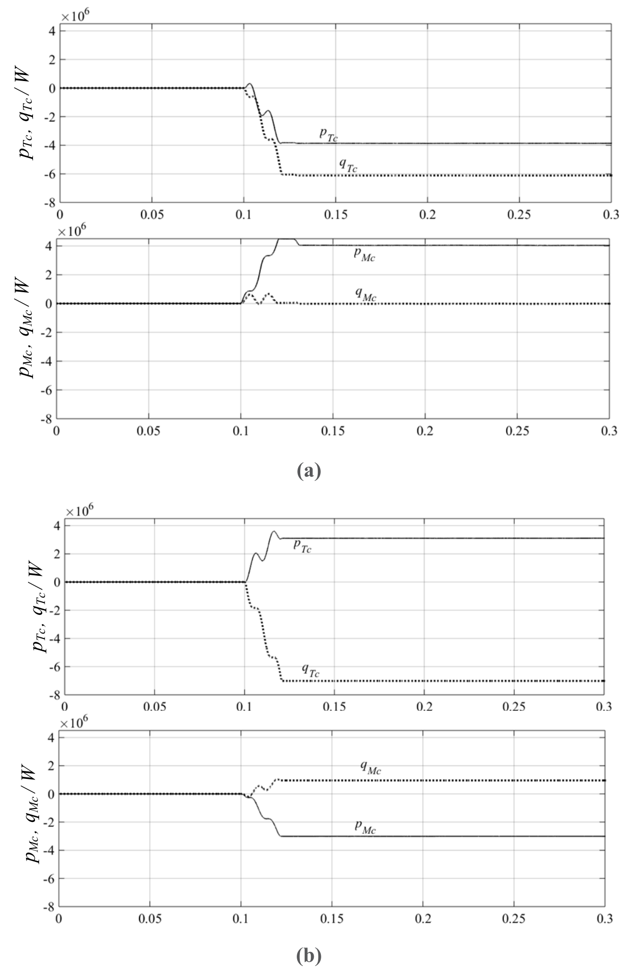

FIGURE 10. The output active and reactive power of case 2 in: (a) ⌞ type structure; (b) ∠ type structure.

1) R LOAD CONDITION

Fig. 11 demonstrates the experimental results with the resistor of 20.8Ω. From Fig. 11(a), it can be concluded that in pure resistive load condition, the compensating current for T phase is completely capacitive and for M phase is purely inductive, but their amplitudes are equal. In this occasion, there is no active current being transferred, this result is consistent with the aforementioned analysis. Fig. 11(b) shows the winding currents of Scott transformer. It can be seen the two secondary currents are equivalent in amplitude and synchronized with each secondary voltages. The compensation performance is satisfied.

TABLE 3. Experimental parameters.

Items	Parameters	Value
Scott transformer	secondary voltage amplitude	90V
Isolation transformer	ratio	90/90
Filter inductance	L_T, L_M	10mH
Capacitance	C_{dc}	3000μF
DC-link	Reference voltage	130V
	Precharge voltage	90V
PI regulator for voltage control	Proportional gain	0.12
	Integral gain	0.0002
Load condition	R	20.8Ω
	RL	15.8Ω+10mH

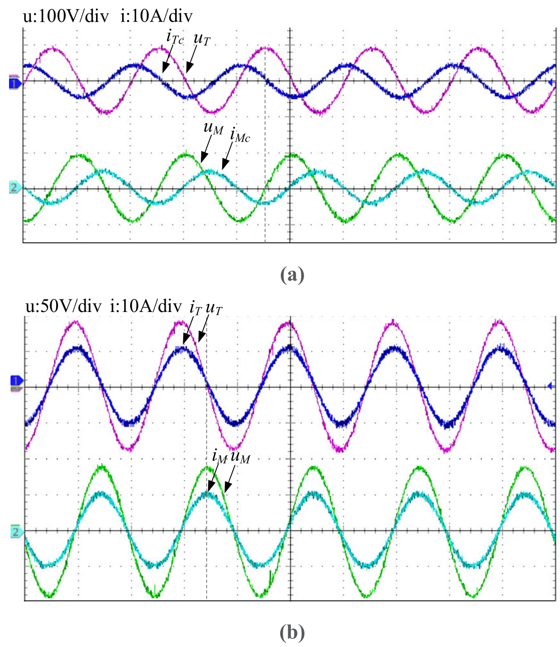

FIGURE 11. Experimental results of R load: (a) secondary voltages and compensating currents of T and M phase; (b) secondary voltages and wingding currents of T and M phase.

2) RL LOAD CONDITION

About the resistive-inductive load, the compensation characteristic is asymmetric. From Fig. 12(a), the amplitude of compensating currents is no longer equal and the phase shifts with corresponding secondary voltages is no longer $\pi/2$ either. For T side, the phase displacement of $\boldsymbol{I}_{Tc}$ is ahead of

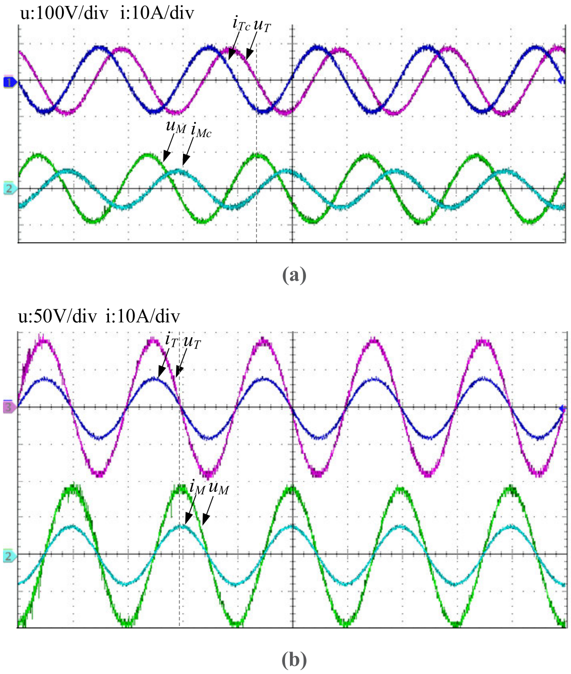

FIGURE 12. **Experimental results of RL load: (a) secondary voltages and compensating currents of T and M phase; (b) secondary voltages and wingding currents of T and M phase.**

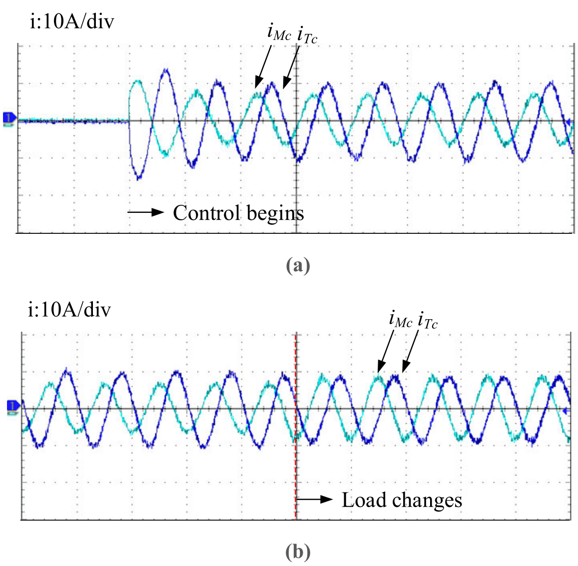

FIGURE 13. **Secondary compensating currents: (a) when the control is implemented; (b) when the load changes from 15.8Ω+10mH to 15.8Ω.**

phase voltage $\boldsymbol{U}_T$ by less $\pi/2$. For M side, the phase angle between $\boldsymbol{I}_{Mc}$ and $\boldsymbol{U}_M$ is lager than $\pi/2$.

Fig. 12(b) shows that winding currents in RL condition are balanced after compensation. Comparing with R condition, the active currents are less due to the smaller active portion of the load.

3) TRANSIENT PROCESS

During the first two periods, compensation system is not activated and the compensating current of T and M port is zero for the time. Then compensation control is enabled from the red line in Fig. 13(a), the system responses quickly to a steady state with load of 15.8Ω+10mH. The slight overshoot is considered to be energy needed for lifting the dc-link voltage from the precharge to the reference value. The Fig. 13 (b) shows the transient process of compensating current of T and M port from the load of 15.8Ω+10mH to the condition of 15.8Ω at the red line. The compensation system quickly converts to another steady state with the equal amplitude of compensating current. The experimental results indicate that the control algorithm can respond to the disturbance in time.

VI. CONCLUSION

This paper proposes a Scott-HPSS to improve the power quality of the electric railway power supply system. Compared with other types of co-phase power supply system, the capacity for active compensation of the Scott-HPSS could be decreased by 29.3%. The voltage rating of compensation devices is reduced by 0.707 in the same condition. In order to further reduce the cost of the system, a partial compensation strategy is proposed based on the power factor and unbalance degree. Then a current detection method is explored and it has a brief arithmetic. The comparative simulations and experiments all verify the feasibility of the proposed system. The results also show that the control algorithm of the Scott-HPSS is reliable and satisfactory.

For practical application, the capacity of Scott transformer in HPSS needs to be investigated overall, such as the maximum phase current, operation arrangement of the loads and the overloading demand of transformer; besides, the modification of winding connection needs to be taken into account as well. Future works also include the establishment of comprehensive control method for cascaded back-to-back converters, such as the balance of dc-link voltages and improvement of current distortion in all range.

REFERENCES

[1] S. L. Chen, R. J. Li, and P. H. Hsi, "Traction system unbalance problem-analysis methodologies," *IEEE Trans. Power Del.*, vol. 19, no. 4, pp. 1877–1883, Oct. 2004, doi: 10.1109/tpwrd.2004.829920.

[2] S. M. Mousavi Gazafrudi, A. Tabakhpour Langerudy, E. F. Fuchs, and K. Al-Haddad, "Power quality issues in railway electrification: A comprehensive perspective," *IEEE Trans. Ind. Electron.*, vol. 62, no. 5, pp. 3081–3090, May 2015, doi: 10.1109/tie.2014.2386794.

[3] R. E. Morrison, K. Warburton, D. J. Young, and D. Hackwell, "The use of static shunt compensation to upgrade existing electrified railways," in *Proc. Int. Conf. Main Line Railway Electrific.*, Sep. 1989, pp. 232–235.

[4] T. Uzuka, "Faster than a speeding bullet: An overview of japanese high-speed rail technology and electrification," *IEEE Electrific. Mag.*, vol. 1, no. 1, pp. 11–20, Sep. 2013, doi: 10.1109/mele.2013.2271839.

[5] T. Uzuka and S. Ikedo, "Railway static power conditioner field test," *Quart. Rep. RTRI*, vol. 45, no. 2, pp. 64–67, 2004, doi: 10.2219/rtriqr.45.64.

[6] T. Uzuka, S. Ikedo, K. Ueda, Y. Mochinaga, S. Funahashi, and K. Ide, "Voltage fluctuation compensator forShinkansen," *Electr. Eng. Jpn.*, vol. 162, no. 4, pp. 25–34, Mar. 2008, doi: 10.1002/eej.20397.

[7] Z. Sun, X. Jiang, D. Zhu, and G. Zhang, "A novel active power quality compensator topology for electrified railway," *IEEE Trans. Power Electron.*, vol. 19, no. 4, pp. 1036–1042, Jul. 2004, doi: 10.1109/tpel.2004.830032.

[8] C. Wu, A. Luo, J. Shen, F. J. Ma, and S. Peng, "A negative sequence compensation method based on a two-phase three-wire converter for a high-speed railway traction power supply system," *IEEE Trans. Power Electron.*, vol. 27, no. 2, pp. 706–717, Feb. 2012, doi: 10.1109/tpel.2011.2159273.

[9] S. Hu, Z. Zhang, Y. Li, L. Luo, P. Luo, Y. Cao, Y. Chen, G. Zhou, B. Wu, and C. Rehtanz, "A new railway power flow control system coupled with asymmetric double LC branches," *IEEE Trans. Power Electron.*, vol. 30, no. 10, pp. 5484–5498, Oct. 2015, doi: 10.1109/tpel.2014.2369132.

[10] N.-Y. Dai, M.-C. Wong, J. M. Guerrero, W.-C. Zhang, and C.-S. Lam, "Analysis, control and experimental verification of a single-phase capacitive-coupling grid-connected inverter," *IET Power Electron.*, vol. 8, no. 5, pp. 770–782, May 2015, doi: 10.1049/iet-pel.2014.0373.

[11] K.-W. Lao, M.-C. Wong, N. Dai, C.-K. Wong, and C.-S. Lam, "A systematic approach to hybrid railway power conditioner design with harmonic compensation for high-speed railway," *IEEE Trans. Ind. Electron.*, vol. 62, no. 2, pp. 930–942, Feb. 2015, doi: 10.1109/tie.2014.2341577.

[12] F. Ma, A. Luo, X. Xu, H. Xiao, C. Wu, and W. Wang, "A simplified power conditioner based on half-bridge converter for high-speed railway system," *IEEE Trans. Ind. Electron.*, vol. 60, no. 2, pp. 728–738, Feb. 2013, doi: 10.1109/tie.2012.2206358.

[13] F. Ma, Z. He, Q. Xu, A. Luo, L. Zhou, and M. Li, "Multilevel power conditioner and its model predictive control for railway traction system," *IEEE Trans. Ind. Electron.*, vol. 63, no. 11, pp. 7275–7285, Nov. 2016, doi: 10.1109/tie.2016.2563379.

[14] F. Ma, Q. Xu, Z. He, C. Tu, Z. Shuai, A. Luo, and Y. Li, "A railway traction power conditioner using modular multilevel converter and its control strategy for high-speed railway system," *IEEE Trans. Transp. Electrific.*, vol. 2, no. 1, pp. 96–109, Mar. 2016, doi: 10.1109/Tte.2016.2515164.

[15] Q. Xu, F. Ma, Z. He, Y. Chen, J. M. Guerrero, A. Luo, Y. Li, and Y. Yue, "Analysis and comparison of modular railway power conditioner for high-speed railway traction system," *IEEE Trans. Power Electron.*, vol. 32, no. 8, pp. 6031–6048, Aug. 2017, doi: 10.1109/tpel.2016.2616721.

[16] S. Hu, B. Wu, C. Rehtanz, Z. Zhang, Y. Chen, G. Zhou, Y. Li, L. Luo, Y. Cao, B. Xie, and X. Chen, "A new integrated hybrid power quality control system for electrical railway," *IEEE Trans. Ind. Electron.*, vol. 62, no. 10, pp. 6222–6232, Oct. 2015, doi: 10.1109/tie.2015.2420614.

[17] Z. Zhang, "Reactive power compensation and negative-sequence current suppression system for electrical railways with YNvd-connected balance transformer—Part I: Theoretical analysis," *IEEE Trans. Power Electron.*, vol. 33, no. 1, pp. 272–282, Jan. 2018, doi: 10.1109/tpel.2017.2670082.

[18] Z. Shu, S. Xie, and Q. Li, "Single-phase Back-To-Back converter for active power balancing, reactive power compensation, and harmonic filtering in traction power system," *IEEE Trans. Power Electron.*, vol. 26, no. 2, pp. 334–343, Feb. 2011, doi: 10.1109/Tpel.2010.2060360.

[19] Z. Shu, S. Xie, K. Lu, Y. Zhao, X. Nan, D. Qiu, F. Zhou, S. Gao, and Q. Li, "Digital detection, control, and distribution system for co-phase traction power supply application," *IEEE Trans. Ind. Electron.*, vol. 60, no. 5, pp. 1831–1839, May 2013, doi: 10.1109/tie.2012.2190959.

[20] K.-W. Lao, M.-C. Wong, N. Y. Dai, C.-K. Wong, and C.-S. Lam, "Analysis of DC-link operation voltage of a hybrid railway power quality conditioner and its PQ compensation capability in high-speed cophase traction power supply," *IEEE Trans. Power Electron.*, vol. 31, no. 2, pp. 1643–1656, Feb. 2016, doi: 10.1109/tpel.2015.2417356.

[21] B. Chen, C. Zhang, C. Tian, J. Wang, and J. Yuan, "A hybrid electrical magnetic power quality compensation system with minimum active compensation capacity for V/V cophase railway power supply system," *IEEE Trans. Power Electron.*, vol. 31, no. 6, pp. 4159–4170, Jun. 2016, doi: 10.1109/tpel.2015.2477459.

[22] B. Chen, G. Xue, W. Zeng, C. Zhang, J. Yuan, and C. Tian, "Electrical magnetic hybrid power quality compensation system for V/V traction power supply system," *IET Power Electron.*, vol. 9, no. 1, pp. 62–70, Jan. 2016, doi: 10.1049/iet-pel.2014.0830.

[23] A. Ghassemi, I. Maghsoud, S. Farshad, and S. S. Fazel, "Comprehensive study on the power rating of a railway power conditioner using thyristor switched capacitor," *IET Electr. Syst. Transp.*, vol. 4, no. 4, pp. 97–106, Dec. 2014, doi: 10.1049/iet-est.2013.0046.

[24] P.-C. Tan, P. C. Loh, and D. G. Holmes, "A robust multilevel hybrid compensation system for 25-kV electrified railway applications," *IEEE Trans. Power Electron.*, vol. 19, no. 4, pp. 1043–1052, Jul. 2004, doi: 10.1109/tpel.2004.830038.

[25] Z. Zhu, F. Ma, X. Wang, L. Deng, G. Li, X. Wei, Y. Tang, and S. Liu, "Operation analysis and a game theoretic approach to dynamic hybrid compensator for the V/v traction system," *IEEE Trans. Power Electron.*, vol. 34, no. 9, pp. 8574–8587, Sep. 2019, doi: 10.1109/tpel.2018.2887226.

[26] B. An, Y. Li, F. Liu, B. Xie, S. Hu, P. Wang, Z. Zhang, L. Luo, and Y. Cao, "An asymmetrical connection balance transformer-based hybrid railway power conditioning system with cost-function optimization," *IEEE Trans. Transp. Electrific.*, vol. 4, no. 2, pp. 577–590, Jun. 2018, doi: 10.1109/tte.2018.2831006.

[27] N.-Y. Dai, K.-W. Lao, M.-C. Wong, and C.-K. Wong, "Modelling and control of a railway power conditioner in co-phase traction power system under partial compensation," *IET Power Electron.*, vol. 7, no. 5, pp. 1044–1054, May 2014, doi: 10.1049/iet-pel.2013.0396.

[28] H. M. Roudsari, A. Jalilian, and S. Jamali, "Flexible fractional compensating mode for railway static power conditioner in a V/v traction power supply system," *IEEE Trans. Ind. Electron.*, vol. 65, no. 10, pp. 7963–7974, Oct. 2018, doi: 10.1109/tie.2018.2801779.

[29] J. Yuan, F. Xiao, C. Zhang, Y. Chen, Z. Ni, and Y. Zhong, "Collaborative unbalance compensation method for high-speed railway traction power supply system considering energy feedback," *IET Power Electron.*, vol. 12, no. 1, pp. 129–137, Jan. 2019, doi: 10.1049/iet-pel.2018.5736.

[30] V. Gelman, "Energy storage that may be too good to be true: Comparison between wayside storage and reversible thyristor controlled rectifiers for heavy rail," *IEEE Veh. Technol. Mag.*, vol. 8, no. 4, pp. 70–80, Dec. 2013, doi: 10.1109/mvt.2013.2283350.

[31] C.-P. Huang, C.-J. Wu, Y.-S. Chuang, S.-K. Peng, J.-L. Yen, and M.-H. Han, "Loading characteristics analysis of specially connected transformers using various power factor definitions," *IEEE Trans. Power Del.*, vol. 21, no. 3, pp. 1406–1413, Jul. 2006, doi: 10.1109/tpwrd.2005.864076.

LEILEI ZHAO (Graduate Student Member, IEEE) was born in Shanxi, China. She received the B.Sc. degree in electrical engineering from Beijing Jiaotong University, Beijing, China, in 2016, where she is currently pursuing the Ph.D. degree. Her research interests include power quality of electric railways and power electronics in traction power supply systems.

MINGLI WU (Member, IEEE) was born in Hebei, China. He received the B.Sc. and M.Sc. degrees in electrical engineering from Southwest Jiaotong University, Chengdu, China, in 1993 and 1996, respectively, and the Ph.D. degree in electrical engineering from Beijing Jiaotong University, Beijing, China, in 2006.

Since 2008, he has been a Professor with the School of Electrical Engineering, Beijing Jiaotong University. His research interests include power supply for electric railways, digital simulation of power systems, and electric power quality.

QIUJIANG LIU (Member, IEEE) was born in Hebei, China. He received the B.Sc., M.Sc., and Ph.D. degrees in electrical engineering from Beijing Jiaotong University, Beijing, China, in 2012, 2014, and 2018, respectively. He is currently a Postdoctoral Researcher with Beijing Jiaotong University. His research interests include power quality of electric railways and power electronics in traction power supply systems.

PENG PENG was born in Henan, China. He received the B.Sc. degree in electrical engineering from Beijing Jiaotong University, Beijing, China, in 2020, where he is currently pursuing the Ph.D. degree. His research interest includes power supply system for electrified railway.

JING LI (Member, IEEE) received the B.Sc. degree in electrical engineering from the North China University of Water Resources and Electric Power, Zhengzhou, China, in 2013, and the M.Sc. degree from Beijing Jiaotong University, Beijing, China, in 2016, where she is currently pursuing the Ph.D. degree in electrical engineering. From October 2018 to 2019, she was a Visiting Student with the Norwegian University of Science and Technology (NTNU), Trondheim, Norway. Her research interests include power quality of electric railways and power electronics in power supply systems.